ELSEVIER

Contents lists available at ScienceDirect

Sensors and Actuators: A. Physical

journal homepage: www.journals.elsevier.com/sensors-and-actuators-a-physical





E-waste resistors-based triboelectric nanogenerators for sustainable energy harvesting and self-powered electronics

B.M. Sankarshan^a, Maruthi Dhiren Palahalli Girigowda^a, S.M. Rumana Farheen^b, L. Adarsh Raj^b, Sebghatullah Amini^b, M.A. Sangamesha^c, S. Krishnaveni^{b,*}

- ^a Department of Physics, The National Institute of Engineering, Mysuru, Karnataka 570008, India
- ^b Department of Studies in Physics, University of Mysore, Mysuru, Karnataka 570006, India
- ^c Department of Chemistry, The National Institute of Engineering, Mysuru, Karnataka 570008, India

ARTICLE INFO

Keywords: E-waste Triboelectric nanogenerators Resistors Energy harvesting Self-powered applications

ABSTRACT

The rapid generation of electronic waste (e-waste) poses a serious environmental challenge, necessitating innovative recycling strategies that add value to discarded materials. In the present work, a novel approach by incorporating recycled waste resistor powders into a polyvinyl alcohol (PVA) matrix to fabricate efficient triboelectric nanogenerators (PR-TENGs) for sustainable energy harvesting and self-powered electronic applications is explored. The impact of varying resistor concentrations and resistance values on the electrical output was systematically investigated. Optimal performance was achieved with a 0.8 g concentration of 1 k Ω resistor powder, yielding a significantly improved output of 224.00 V and 7.03 μ A compared to plain PVA. Detailed material characterization of PR composite film from optimized device via SEM, EDS, PXRD, and FTIR revealed that the enhanced triboelectric generation is attributed to modifications in the composite's surface roughness, elemental composition, crystallinity, and functional group interactions induced by the resistor fillers. The energy harvesting capability of the optimized PR-TENG was further demonstrated through efficient charging of capacitors. Proof-of-concept applications, including powering a calculator, illuminating LEDs, and self-powered biomechanical sensor, highlight the potential of this approach for sustainable energy harvesting using recycled electronic waste.

1. Introduction

In recent years, the rapid advancement of electronic devices has resulted in an alarming accumulation of electronic waste (e-waste), posing significant environmental and health challenges [1]. In 2010, the world generated 3.4 billion kg of e-waste, an amount that has since increased annually by an average of 2.3 billion kg. Also, the documented formal collection and recycling rate has increased as well, growing from 8 billion kg in 2010 at an average rate of 0.5 billion kg per year to 13.8 billion kg in 2022 [2]. E-waste contains valuable materials, including metals, plastics, and semiconductor components, which, if not properly managed, contribute to environmental pollution and resource depletion [3]. To address these challenges, researchers have explored innovative methods for repurposing e-waste, one of which is the development of e-waste-based triboelectric nanogenerators (E-TENGs). TENGs, first introduced by Wang et al. in 2012, are energy-harvesting devices that convert mechanical energy into electrical energy through the

triboelectric effect and electrostatic induction [4–6]. These devices have garnered significant interest due to their cost-effectiveness, high efficiency, and ability to harness energy from ambient mechanical sources such as vibrations, human motion, and wind [7].

E-waste, comprising discarded devices like smartphones, laptops, batteries, and circuit boards, contains a wealth of functional materials that can be effectively repurposed into energy harvesting systems. Several pioneering studies have highlighted the feasibility and effectiveness of utilizing e-waste for TENG fabrication. Ahmed et al. [8] successfully repurposed smartphone display layers from various brands into TENGs housed within recycled PET bottles, achieving a peak voltage of 190.31 V and a current of 9.56 μA through biomechanical energy harvesting. In another approach, graphite recovered from waste dry cells was mixed with pen gel ink to develop conductive electrode pastes for TENGs, resulting in outputs of 83.88 V and 101.00 μA [9]. Additionally, Zhang et al. [10] recycled spent lithium iron phosphate batteries (LIBs) to construct wind-driven TENGs using extracted casings,

E-mail address: sk@physics.uni-mysore.ac.in (S. Krishnaveni).

^{*} Corresponding author.

films, and metals, which not only harvested energy but also powered electrochemical recycling systems. Furthermore, Natarajan et al. [11] demonstrated a comprehensive recycling strategy by transforming LIB components into high-performance graphene-based supercapacitors, catalysts, and TENGs. Zhao et al. [12] also innovatively employed ground resistive and IC elements from waste PCBs to develop positive triboelectric layers for energy harvesting. These studies collectively highlight the immense potential of using e-waste as a valuable resource for sustainable energy applications. In this context, integrating e-waste materials into TENG fabrication represents a synergistic approach to address two critical global challenges: electronic waste management and sustainable energy generation. Despite this progress, most prior studies have focused on using conductive or semiconducting e-waste materials such as graphite or metals for electrode or structural components. The potential of resistors, particularly those with ceramic bodies as triboelectric materials remain largely underexplored.

Resistors, one of the most abundant components in discarded electronic devices. Waste resistors can be sourced from a variety of discarded and obsolete electronic devices that are abundant in today's e-waste streams. Common sources include broken or outdated consumer electronics such as televisions, radios, computers, laptops, printers, mobile phones, and gaming consoles, where resistors are present on the internal circuit boards. Industrial and commercial equipment like control panels, communication devices, and manufacturing machinery also yield significant quantities of resistors when decommissioned [13]. Additionally, educational institutions and research labs frequently dispose of old experimental setups and electronic kits containing reusable resistors. Repair shops, electronic service centres, and recycling facilities are important hubs where waste resistors can be collected, as they routinely discard damaged PCBs and failed components. Recycling waste resistors can be approached through several methods, depending on whether the goal is material recovery or functional reutilization in secondary applications. For material recovery, resistors are subjected to processes like thermal treatment, chemical leaching, and mechanical separation [14, 15]. Alternatively, waste resistors can be directly reused, particularly when designing devices like TENGs. Resistors, are composed of ceramic-metal composites such as ruthenium oxide (RuO2), tin oxide (SnO₂), nickel oxide (NiO) embedded in a ceramic binder matrix like aluminum oxide (Al₂O₃) and silicon dioxide (SiO₂) [16,17], which tend to be good triboelectric materials, but have remained largely unexplored for TENG applications. Also, ceramics like alumina possess high dielectric constants and low charge dissipation, which enhance charge accumulation during triboelectric interactions [18]. Moreover, resistor-derived ceramics yield comparable or improved performance due to their composite nature (ceramic core, metal oxide coatings), which may enhance surface polarization and interfacial charge trapping [19]. Thus, recycling resistors as active triboelectric layers can offer not only an economical pathway for device fabrication but also contribute to the broader circular economy by extending the functional life of waste components.

The present study reports the design, fabrication, and characterization of PVA polymer and e-waste resistor-based triboelectric nanogenerators (PR-TENGs). By employing resistors sourced from discarded electronic boards, broken and outdated consumer electronics into the PVA matrix to prepare PVA-Resistors (PR) composite films. The asobtained PR composite films with varying concentration of grinded resistors were employed as tribopositive material, FEP as tribonegative material to fabricate PR-TENGs. The PR composite film from the optimised device is subjected to various analytical techniques to study the surface and functional characteristics. Further optimized PR-TENG is evaluated for its application in driving low-power electronic devices such as charging capacitors, powering LEDs, and charging digital calculator. The results not only reinforce the viability of using recycled electronic components in energy-harvesting systems but also open new avenues for sustainable, low-cost, and eco-friendly TENG technologies. This work underscores the role of material innovation in building a

circular energy economy, where waste is transformed into a valuable resource for the next generation of green electronics.

2. Experimental section

2.1. Materials

Laboratory-grade distilled water, polyvinyl alcohol powder (molecular weight = 125,000) purchased from Otto Chemie Pvt. Ltd., Mumbai, Maharashtra. Waste-resistors of various resistance values (1k, 10k, 100k, and 470k) collected from discarded electronic boards, broken and outdated consumer electronics. Commercially purchased aluminium foil adhesive tape; and multi-strand copper wires were used.

2.2. Preparation of PVA-resistors composite solution

The schematic illustration of the PR composite solution preparation is provided in Fig. 1(a) & (b). The PR composite film was prepared in the following steps: Resistors were grinded to fine powder using mortar and pestle. 100 ml of DI water is taken in a beaker and heated to 60 °C. For the hot DI water, 7 g of PVA powder is added slowly and stirred thoroughly with a magnetic stirrer for about 15 min to get 7 % PVA solution. Further, 0.05, 0.1, 0.2, 0.4 and 0.8 g of resistor powder is added and mixed with 20 ml each solution of PVA for 10 min. The solution was cast by pouring it into a Petri dish and dried for two days.

2.3. PR-TENG fabrication

The dried films were peeled off and utilized in the fabrication of TENG. The schematic representation for the device fabrication is provided in Fig. 1(c). PR composite film was used as tribopositive layer and FEP film was used as tribonegative layer due to its strong negative electron affinity [20]. Both the layers were cut with the dimension of 4×4 cm² and pasted on Al foil tape which acts as the electrodes of the device. Two conducting wires were used to connect the Al electrodes to an external load for electrical measurements. A portion of the waste-water bottle made of PET polymer was cut horizontally with the dimension of $6 \times 10 \text{ cm}^2$. The triboelectric layers of the device were pasted into the inner surface of the water bottle to bring them into an arch-shape structure so that the device was designed in a vertical contact-separation mode, where periodic mechanical contact between the triboelectric layers results in transfer of charges between them. The insulating nature of the PET water bottle effectively prevents charge leakage. Also, the plastic water bottle was used as a substrate to increase the mechanical durability of the frictional layers and electrodes of the devices. The inter-layer separation distance was maintained to be 2 cm.

2.4. Characterization and electrical measurements

The PR composite films were thoroughly characterized using various analytical techniques to evaluate their structural, chemical, and electrical properties. The surface morphology and elemental composition of pristine PVA and PR composites were studied using Scanning electron microscopy (SEM) combined with energy-dispersive X-ray spectroscopy (EDS) (Zeiss, EVOLS15, Germany). Dielectric studies were done using capacitance measurement with varying frequency from 4 to 800 kHz (Hioki LCR Meter, Model: IM3536, Japan). To analyse the chemical interactions and detect the functional groups present in the materials, Fourier transform infrared spectroscopy (FTIR, JASCO 4100, Japan) was used. For electric performance evaluation, the voltage and current outputs of the PR-TENG devices were measured using a source measurement unit (SMU) (Keithley, Model 2460, USA). Furthermore, the long term stability and mechanical durability of the fabricated device were assessed using a custom built linear motor system under repeated operation.

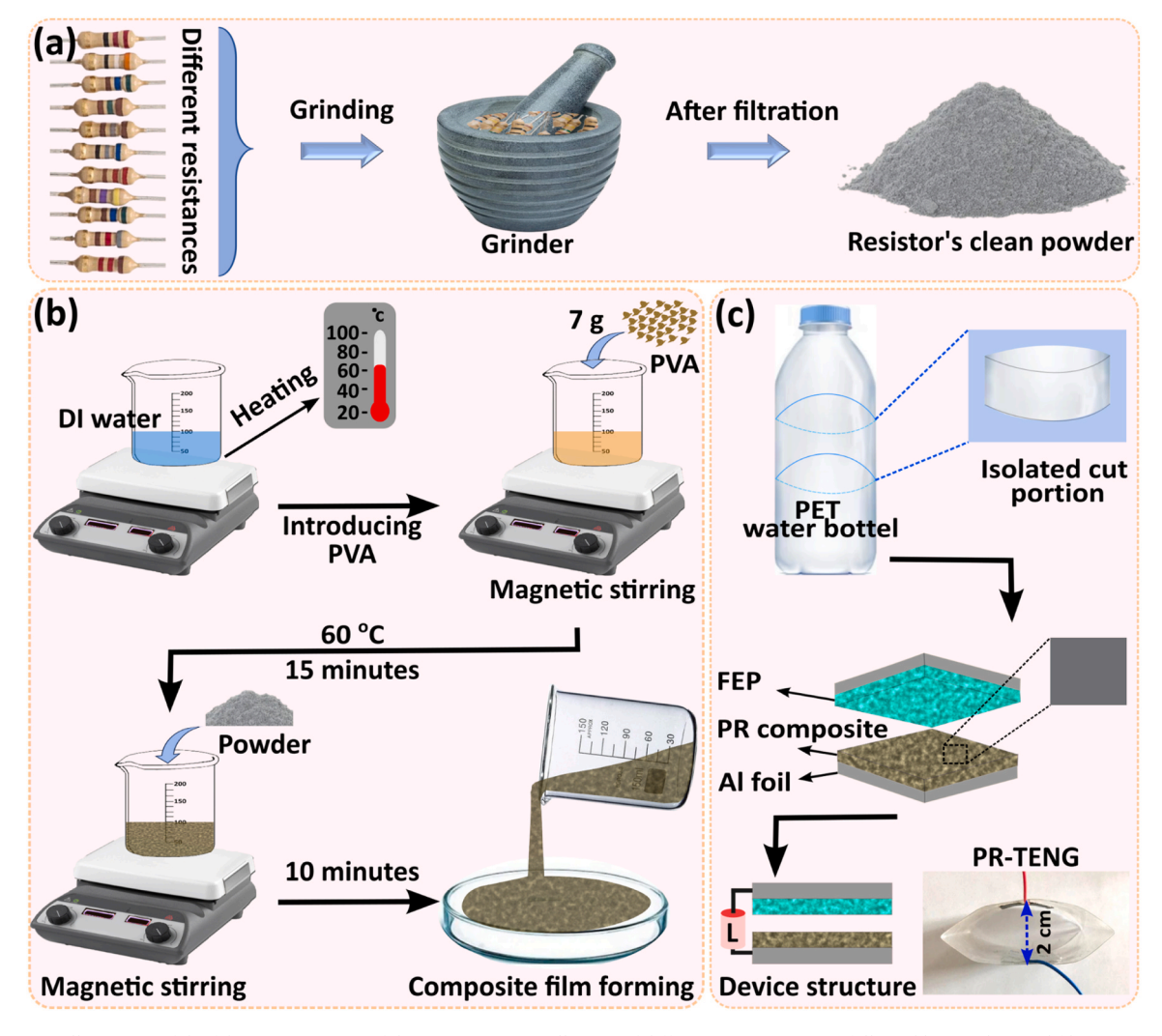


Fig. 1. Schematic illustration of the fabrication process of the PR-TENG: (a) Collection of different waste resistors, followed by grinding and filtration to obtain clean resistor powder. (b) Preparation of the PR-polymer composite film. (c) Fabrication of the PR-TENG device along with a depiction of the complete device structure.

3. Results and discussions

3.1. Working mechanism of PR-TENGs

The working mechanism of the PR-TENGs operates on the contactseparation mode principle, utilizing the triboelectric effect and electrostatic induction to generate electrical signals. Initially, in the resting state (Fig. 2(a)), the PR composite layer and the FEP film are separated by a small distance, and no charge transfer occurs, resulting in no current flow in the external circuit. When an external force is applied, the two surfaces come into intimate contact, leading to charge transfer based on their differing triboelectric polarities (Fig. 2b). The PR composite acts as the electron-donating layer, while the FEP film behaves as the electron-accepting layer. After maximum contact, surface charges of opposite signs accumulate on the contacting surfaces, but no current is generated yet as there is no separation. Upon releasing the external force, the two layers begin to separate (Fig. 2c), and the electrostatic field generated by the separated charges drives the free electrons through the external circuit. This results in a positive current peak as the potential difference builds up. When the layers are fully separated (Fig. 2d), the system reaches the maximum potential difference, and the current returns to zero since there is no further movement. Subsequently, when a pressing force is reapplied (Fig. 2e), the layers move back toward each other, causing electrons to flow in the opposite direction, generating a negative current peak. This alternate movement of pressing and releasing results in alternating current (AC) generation. Finally, when the layers are completely pressed together again (Fig. 2f), the system returns to a state of no current flow, completing one full cycle. Thus, the PR-TENG continuously generates AC electrical signals in response to mechanical motions through cyclic contact and separation between the PR composite and FEP surfaces, enabling sustainable energy harvesting.

3.2. Electrical output performance of PR-TENGs

The electrical output performance of PR-TENGs was systematically evaluated under controlled mechanical stimuli. When subjected to periodic pressing and releasing cycles at 5 Hz, the PR-TENG exhibited distinct alternating current signals characterized by sharp positive and negative peaks, corresponding to the contact-separation motions. The performance optimization of the PR-TENGs were carried out by systematically varying the concentration of resistor (R) powders within the PVA matrix and evaluating their effects on electrical output characteristics (Table 1). Fig. 3(a–d) illustrates the variation of voltage (red bars) and circuit (blue bars) for different resistor values (R = 1 k Ω , 10 k Ω , 100 k Ω , and 470 k Ω) as a function of R-concentration. For the 1 k Ω resistor-based PR-TENG (Fig. 3a), an increase in resistor concentration from 0 to 0.8 g led to a gradual improvement in voltage and current outputs, with maximum values observed around 0.8 g. Similarly, for the 10 k Ω resistor (Fig. 3b), the PR-TENG showed a peak performance at 0.2 g

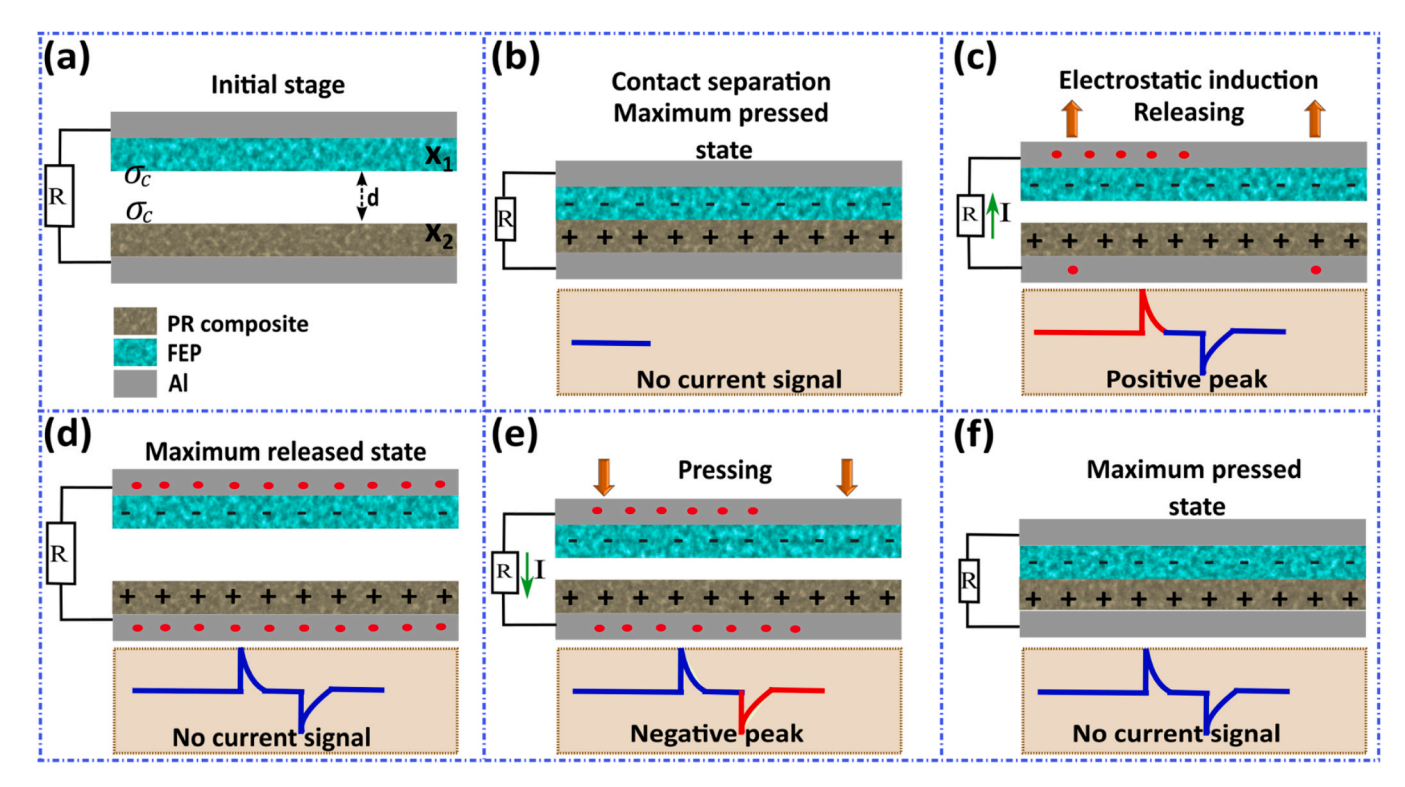


Fig. 2. Working mechanism of PR-TENG. (a) Initial separated state. (b) Maximum contact with charge transfer but no current. (c) Releasing generates a positive current peak. (d) Maximum separation with no current. (e) Pressing induces a negative current peak. (f) Return to maximum contact state.

Table 1Output performance of PR-TENGs.

R-filler conc. (g)	PR-TENGs							
	1k		10k		100k		470k	
	Voltage (V)	Current (µA)						
0.05	184.93	2.93	146.37	3.36	162.37	3.84	160.94	3.80
0.1	198.85	2.25	156.02	4.64	170.26	1.92	180.29	2.90
0.2	202.53	2.86	172.47	4.92	186.36	2.72	204.04	3.13
0.4	210.85	6.67	166.74	3.18	196.85	1.55	170.17	3.58
0.8	224.00	7.03	124.07	3.95	218.95	2.34	146.87	3.37

concentration. In the case of the 100 $k\Omega$ resistor-based device (Fig. 3c), the voltage and current outputs increased steadily with concentration up to 0.8 g. For the 470 $k\Omega$ resistor-based PR-TENG (Fig. 3d), the optimal performance was achieved at 0.2 g concentration, beyond which both voltage and current outputs started to decrease. Thus, the higher filler contents beyond the optimal point likely lead to agglomeration, poor mechanical integrity, and reduced surface charge generation, adversely affecting device performance. Therefore, careful tuning of resistor concentration is crucial for enhancing the energy harvesting capabilities of PR-TENGs.

The Fig. 4 comprehensively illustrates the enhanced electrical performance of the PR-TENGs when compared to the plain PVA device. In Figs. 4(a) and 4(b), the voltage and current output profiles are presented for different composite concentrations (0.2 g and 0.8 g) using various resistor types (1 k Ω , 10 k Ω , 100 k Ω , and 470 k Ω). It is evident that the incorporation of resistor powders into the PVA matrix significantly boosts the voltage and current outputs compared to the plain PVA device. Specifically, the plain PVA device exhibited a voltage of 132.00 V and a current of 3.12 μ A. However, the PR-TENGs with optimized resistor content showed much higher outputs. At 1 k Ω resistors powder with 0.8 g R-concentration, the PR-TENG achieved a high output of 224.00 V and 7.03 μ A, indicating that the addition of resistive materials effectively improves the dielectric and surface properties, facilitating

more efficient charge separation and transfer during triboelectric operations [21,22]. All resistors, along with their ceramic coatings, were finely ground and uniformly blended into the PVA matrix, forming composites with distinct electrical and structural characteristics. However, the different resistor values (1, 10, 100, 470 k Ω) lead to varying electrical outputs in PR-TENGs due to differences in internal conductivity, charge transfer efficiency, and dielectric behavior introduced by each filler [23]. Low-resistance fillers (e.g., 1 k Ω) enhance conductivity and facilitate efficient charge transport, resulting in higher current and voltage outputs, especially at optimized concentrations (0.8 g). In contrast, high-resistance fillers (e.g., 470 k Ω) limit charge mobility due to greater internal resistance, yielding lower outputs beyond their optimal concentration of 0.2 g. Additionally, the ceramic coating contributes to surface polarization and dielectric enhancement but excessive filler content leads to agglomeration and poor performance [24]. Thus, the electrical output is a result of the balance between conductive pathways and dielectric contrast influenced by the resistor value and concentration.

The device composed of 1 k Ω resistors with 0.8 g R-concentration was considered as the optimised device, which was further used for other electrical measurements and demonstrating applications. Fig. 4(c) demonstrates the dependence of the PR-TENG's electrical output on the applied mechanical force. Both the voltage and current outputs increase

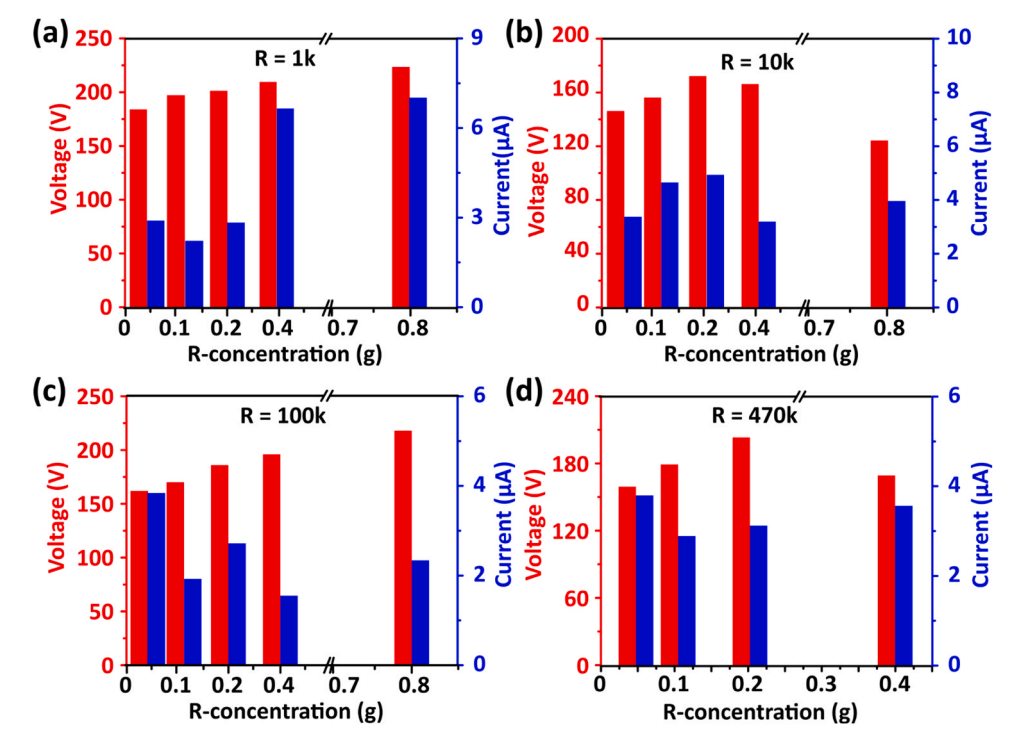


Fig. 3. Electrical output performance of PR-TENGs with varying resistor (R) concentrations: (a) $R=1~k\Omega$, (b) $R=10~k\Omega$, (c) $R=100~k\Omega$, and (d) $R=470~k\Omega$. The peak-to-peak voltage (red bars) and current (blue bars) as functions of R-concentration.

with increasing force, indicating that the PR-TENGs are highly sensitive to mechanical stimuli. Specifically, under an applied force of 12 N, the PR-TENG generated an output voltage of approximately 224.00 V and a current of $7.03~\mu A$. The insets in Fig. 4(c) show real-time output profiles under varying forces, This behavior can be attributed to the enhanced contact intimacy between the triboelectric layers under higher forces, leading to greater output voltage and current during the contact-separation cycles [25,26].

Fig. 4(d) investigates the electrical performance of the PR-TENG by examining its output voltage and current in response to varying external load resistances. The load resistances were varied from 1 to 250 M Ω , and the corresponding generated output voltage and the current was measured. The trends reveal an inverse relationship between these two parameters: as the load resistance increases, the output voltage across it tends to rise, characteristic of a high-impedance source, whereas the output current correspondingly diminishes, adhering to Ohm's Law [27, 28]. The insets provide a visual representation of the circuit diagram, illustrating the PR-TENG connected to an external resistor under the influence of an external mechanical force. The data presented in this figure is fundamental for understanding the electrical characteristics of the PR-TENG and for subsequently determining the optimal load resistance that maximizes power transfer, a relationship likely explored in greater detail in Fig. 4(e). The observed behavior underscores the nature of TENGs as high-impedance voltage sources, capable of producing significant voltages, particularly under high resistance conditions, but with a limitation on the deliverable current, especially at higher loads [29,30].

Fig. 4(e) elucidates the maximum power generation against a range of external load resistances from 1 to 250 M Ω . The graph reveals a distinct peak, indicating the existence of an optimal load resistance at which the device delivers maximum power. Specifically, the data shows a peak power output of 1.78 mW achieved when the load resistance is 90 M Ω , as calculated using P = I²R. At very low load resistances, despite higher current, the low voltage results in low power output, while at very high resistances, the high voltage is offset by a significantly reduced current, again leading to low power. The identification of this optimal

load resistance is of paramount importance for practical applications, as operating the TENG at this specific resistance ensures the most efficient conversion of mechanical energy into electrical energy [31,32].

Finally, Fig. 4(f) presents the durability and stability of the PR-TENG over continuous mechanical cycling for 12,000 cycles. The graph clearly demonstrates that the output voltage remains remarkably consistent and stable throughout the entire testing period. The repetitive peaks in the voltage waveform indicate the consistent generation of electrical energy with each cycle of mechanical input emphasizing the sustained and reliable performance of the PR-TENG without significant degradation over extensive use. This long-term stability is a crucial factor for the practical viability of energy harvesting devices. This high durability ensures the potential of PR-TENGs for practical energy harvesting applications, where prolonged mechanical operation is required. Thus, the integration of waste resistor powders into the PVA matrix substantially improves the triboelectric performance of the devices.

3.3. Analyses of PR composite films from the optimized device

Based on the characterization results presented in Fig. 5(a) to (d), the higher output performance of the PR-TENG incorporating resistor powders (specifically the optimized 0.8 g concentration with likely 1 k Ω characteristic influencing the composite formation) compared to the plain PVA device can be attributed to a synergistic effect of changes in surface morphology, elemental composition, crystallinity, and functional groups.

The SEM images provide a visual comparison of the surface morphology of pristine PVA film and PR composite film with 1 $k\Omega$ resistors, 0.8 g filler concentration. The SEM images in Fig. 5(a) reveal surface morphology of PVA film, which exhibits a smooth and homogeneous surface, while the composite films display a distinctly textured surface characterized by the dispersion of particles within the PVA matrix. This altered surface morphology is directly linked to the enhanced performance of the PR-TENG at a 0.8 g filler concentration with 1 $k\Omega$ resistor powder. The increased surface roughness, resulting from the embedded filler, increases the effective contact area during

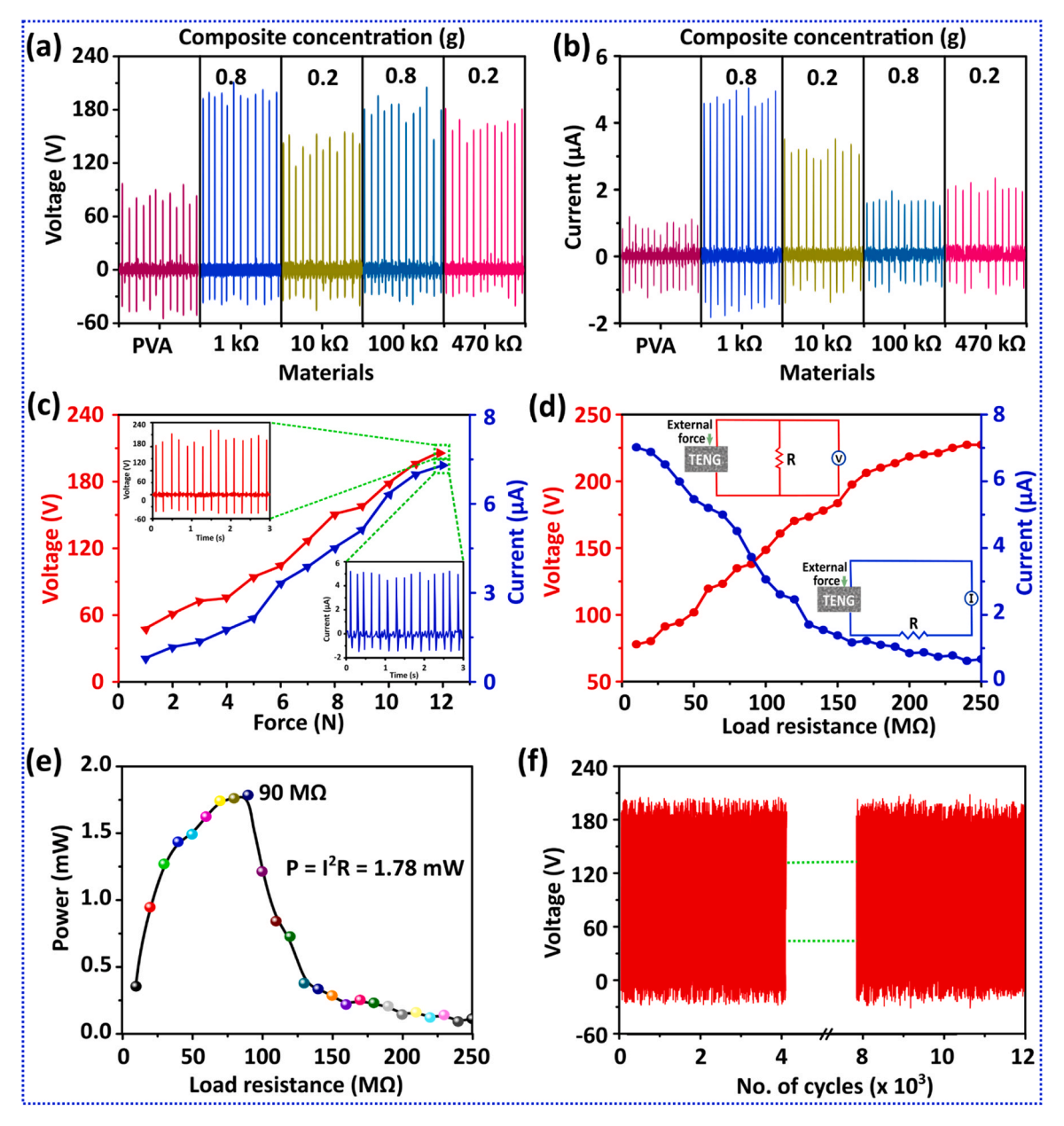


Fig. 4. Electrical characterization of optimized PR-TENG. (a) Voltage and (b) current outputs of PR-TENGs with different composite concentrations and resistor types compared to plain PVA. (c) Output performance versus applied force (insets: real-time signals). (d) Voltage and current variations with load resistance (inset: circuit diagram). (e) Power optimization showing maximum power at 90 M Ω . (f) Stability test over 12,000 cycles.

triboelectric interaction, leading to greater charge accumulation [33]. Fig. 5(b) presents EDS spectra and accompanying elemental composition tables for a pristine PVA film and a PR composite film (1 kΩ). The EDS spectrum for PVA primarily shows prominent peaks corresponding to Carbon (C) and Oxygen (O), which are the constituent elements of the PVA polymer. The elemental composition table for PVA indicates a weight percentage and atomic percentages of the elements, respectively. Compared to the pristine PVA film, which primarily consists of carbon (53.6 wt%) and oxygen (46.4 wt%), the resistorintegrated composites exhibit additional elements such as Na (1.1-2 wt%), Al (up to 0.9 wt%), Si (0.7-1.1 wt%), and trace Mg (0.9 wt %), depending on the resistance value (Table S2. supporting information). These elements, likely originating from the ceramic coatings of resistors, introduce surface heterogeneity and charge trapping sites [34, 35], that are not present in the base PVA, suggesting a role of elemental doping in enhancing surface polarization and charge retention. For instance, the 1 $k\Omega$ composite contains higher levels of Sodium (Na),

Aluminum (Al), and Silicon (Si) compared to others, correlating with its superior electrical output. The presence and relative amounts of these additional elements provide crucial information about the composition of the PR composite and its potential impact on the material's triboelectric and electrical characteristics, which are relevant to its performance in the PR-TENG device.

Figure S3 presents the frequency-dependent dielectric behavior of PR composites, highlighting the influence of both resistor type (1, 10, 100, and 470 k Ω) and filler concentration (0.05. 0.1, 0.2, and 0.4 g). In Figure S 3a (Supporting Information), all resistor-filled composites exhibit a higher dielectric constant than pristine PVA, with the 470 k Ω PR composite demonstrating the highest dielectric constant across the frequency range of 4–800 kHz, followed by 100 k Ω , 10 k Ω , and 1 k Ω . This enhancement is attributed to increased interfacial polarization introduced by the ceramic components in the resistors [36]. The dielectric constant decreases with increasing frequency due to reduced dipolar orientation at higher frequencies, a typical response in

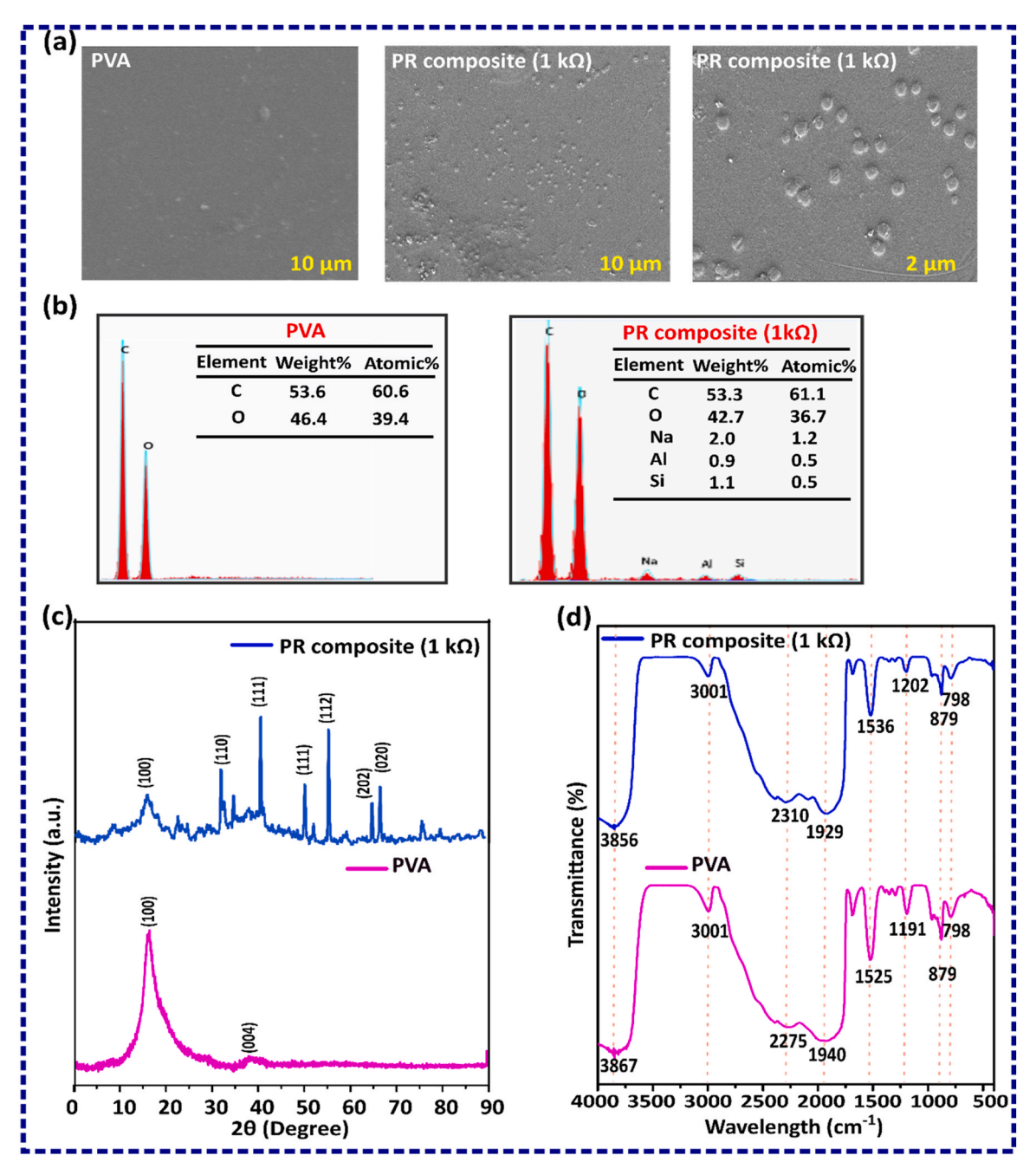


Fig. 5. Characterization of PR-film from optimized device. (a) SEM Analyses, (b) EDS spectra and elemental composition tables, (c) PXRD patterns, and (d) FTIR spectra of pristine PVA film and PR composite film (1 $k\Omega$).

polymer-based dielectrics [37]. Figure S 3b (Supporting Information) shows the effect of varying filler concentration in the $1~k\Omega$ PR composite, where the dielectric constant increases with concentration up to 0.4 g, indicating enhanced polarization and filler dispersion [38]. These trends confirm that both the type and concentration of resistor fillers critically modulate the dielectric properties of the composite, directly influencing the triboelectric performance of PR-TENGs.

Figure S2 (Supporting Information) represents the PXRD profile of powdered resistors (1, 10, 100, and 470 k Ω). To study the influence of material crystallinity on triboelectric performance, crystallite sizes of ground resistor powders with different resistance values were estimated using Scherer's method [39]. The calculated crystallite sizes were found to be 11.38 nm for 1 k Ω , 32.81 nm for 10 k Ω , 23.29 nm for 100 k Ω , and 50.91 nm for 470 k Ω . Among these, the 1 k Ω sample exhibited the smallest crystallite size, which is expected to offer a larger surface area

and higher density of active sites for charge generation, contributing to its superior electrical output [40]. Conversely, the larger crystallite size in the 470 k Ω sample may reduce surface activity, correlating with its comparatively lower performance [41]. Fig. 5(c) presents the PXRD patterns for both a pristine PVA film and a PR composite film (1 k Ω). The PXRD pattern of the PVA film exhibits broad, less intense peaks, notably a prominent broad halo centered around $2\theta=19.8^\circ$, which is characteristic of the semi-crystalline nature of PVA, indicating regions of ordered and disordered polymer chains [42]. Additionally, a very weak and broad peak is observed around $2\theta\approx40.63^\circ$, corresponding to the (004) plane [43]. In contrast, the PXRD pattern of the PR composite (1 k Ω) displays numerous sharp and well-defined diffraction peaks superimposed on a broader background. These sharp peaks indicate the presence of crystalline phases within the composite material, which are absent in the pristine PVA. The Miller indices (e.g., 110, 111, 112, 202,

and 020) are labelled for several of these distinct peaks, providing information about the crystallographic planes of the incorporated filler material within the PVA matrix. The presence of these sharp peaks confirms the successful incorporation of a crystalline filler into the PVA, leading to a composite material with a significantly different structural order compared to the semi-crystalline PVA [44]. This change in crystallinity and the introduction of specific crystalline phases due to the

filler are likely to influence the mechanical, electrical, and ultimately the triboelectric properties of the PR composite.

Fig. 5(d) presents the FTIR spectra of both pristine PVA and the PR composite (1 k Ω) film. The FTIR spectrum of PVA exhibits characteristic absorption bands associated with its functional groups: a broad band around 3001–3867 cm⁻¹ attributed to O-H stretching vibrations, a peak at approximately 2940 cm⁻¹ corresponding to C-H stretching [45], a

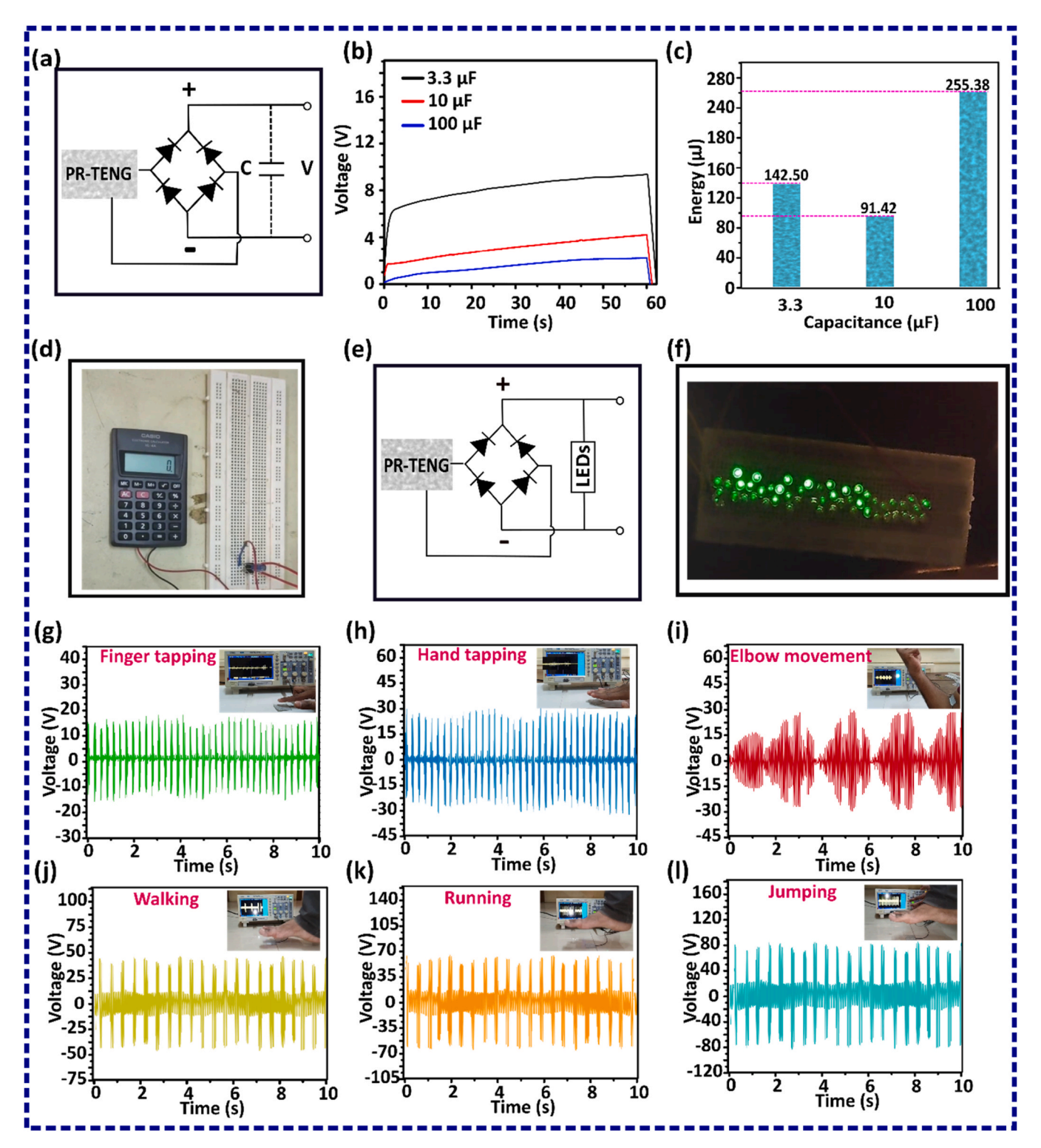


Fig. 6. (a) Circuit diagram for charging capacitor. (b) Charging curves for different capacitors. (c) Energy stored in different capacitors. (d) Photograph of powering digital calculator. (e) Circuit diagram for powering LEDs. (f) Photograph of powering LEDs. PR-TENG as a self-powered biomechanical sensor for (g) Finger tapping, (h) Hand tapping, (i) Elbow movement, (j) Walking, (k) Running and (l) jumping.

peak near 1420 cm⁻¹ due to C-H bending [46], a band around 1090 cm⁻¹ assigned to C-O stretching [47], and a peak around 830 cm⁻¹ related to C-C stretching [48]. The FTIR spectrum of the PR composite (1 $k\Omega$) shows several similarities to that of PVA, indicating the presence of the PVA matrix. However, it also displays distinct differences, suggesting the incorporation of the filler material. Notably, there are shifts in the positions and intensities of some characteristic PVA peaks, such as the O-H stretching band shifting to around 3001-3856 cm⁻¹ and the C-O stretching region showing alterations. Additionally, the appearance of new peaks or changes in the fingerprint region (below 1500 cm⁻¹) at wavenumbers like 1536 cm⁻¹, 1202 cm⁻¹, and potentially subtle changes around 798 and 879 cm⁻¹ indicate the presence of specific functional groups or vibrational modes associated with the incorporated filler material likely containing the elements Na, Al, and Si identified in the EDS analysis. These changes in the FTIR spectrum of the PR composite confirm the successful incorporation of the filler within the PVA matrix. Also, the alterations suggest potential chemical interactions between the PVA matrix and the resistor powders, which can modify the surface energy and charge trapping sites, thereby facilitating more efficient triboelectric charge generation and retention, ultimately leading to higher voltage and current outputs [49]. The SEM, EDS, XRD and FTIR of the PR composite film of 10, 100, and 470 k Ω resistors have been included in the Figure S1, Supporting information.

4. Applications of optimized PR-TENG

The energy harvesting and storage capabilities of the optimized PR-TENG is illustrated in Fig. 6. The schematic circuit designed for capturing and storing the electrical energy generated by the PR-TENG is shown in Fig. 6(a). The setup begins with the PR-TENG, which produces an alternating current (AC) output. This AC power is then fed into a fullwave rectifier, an arrangement of four diodes that efficiently converts the bi-directional AC into a unidirectional direct current (DC). Following the rectifier, a capacitor (C) is connected in parallel. This capacitor serves as the energy storage element, accumulating the electrical charge supplied by the rectified output of the PR-TENG. Finally, the voltage (V) developed across the capacitor is measured to quantify the amount of energy stored within it. This graph in Fig. 6(b) illustrates the voltage characteristics across capacitors of varying capacitances (3.3 μF , 10 μF , and 100 $\mu F)$ as they are charged by the PR-TENG over a period of 60 s under consistent mechanical stimulation by hand tapping. Notably, the capacitor with the smallest capacitance, 3.3 µF, exhibits the most rapid increase in voltage, reaching the highest value within the given timeframe. Conversely, as the capacitance increases to 10 µF and further to $100 \mu F$, the rate of voltage accumulation slows down, and the final voltage obtained within the 60 s is progressively lower. This behavior is consistent with the fundamental relationship between charge, capacitance, and voltage, where larger capacitors require more charge to achieve the same voltage [50]. The bar graph in Fig. 6(c) quantifies the electrical energy stored in capacitors of different capacitances (3.3 µF, 10 μF, and 100 μF) after being charged by the PR-TENG for 60-second charging period shown in Fig. 6(b). The stored energy is calculated using the formula $E = \frac{1}{2} CV^2$ (Note S1, Supporting information). Despite the 100 µF capacitor exhibiting a lower voltage compared to the smaller capacitances, it ultimately stores the largest amount of energy (255.38 $\mu J)$ due to its significantly higher capacitance value and the quadratic dependence of energy on voltage. The 3.3 μF capacitor stores 142.50 μJ , while the 10 µF capacitor stores 91.42 µJ. This demonstrates that for maximizing energy storage, a larger capacitance is more beneficial, even if it charges to a lower voltage within a given timeframe, due to its greater capacity to hold charge.

The Fig. 6(d) presents a real-world demonstration of the energy harvesting and storage potential of the PR-TENG. The photograph shows a calculator displaying "0" alongside a breadboard containing the rectifier circuit, with connections implied to the PR-TENG (Supporting Video S1). This setup suggests an experiment where the electrical energy

generated by the PR-TENG is rectified and stored in a capacitor, and this stored energy in $3.3 \, \mu F$ is then utilized to power the calculator. While the image only shows the initial state of the calculator, it implies the successful transfer and utilization of the harvested energy to operate a small electronic device. The Fig. 6(e) illustrates another application of the PR-TENG as a direct power source. The schematic diagram shows the PR-TENG connected to a full-wave rectifier, DC power is then directly used to drive a series of Light Emitting Diodes (LEDs) connected in a circuit. The photograph in Fig. 6(f) provides visual evidence of the circuit depicted in Fig. 6(e) in operation. Around 65 green LEDs are shown illuminated, emitting light (Supporting Video S2). This confirms that the electrical energy generated by the PR- TENG is sufficient to directly power and light up these LEDs. This successful demonstration highlights the potential of the PR-TENG as a self-sustaining power source for smallscale electronic devices, showcasing its ability to convert mechanical energy into usable electrical energy for practical applications [51–54]. Further, the optimized PR-TENG device is employed as a biomechanical energy harvester, which showcases the device's capability to effectively harvest energy from human motion such as finger tapping, hand tapping, elbow movement, walking, running and jumping and convert it into usable electrical output. As shown in Fig. 6(g-l), distinct voltage signals were recorded for each motion type, indicating reliable and sensitive energy generation. The device generated peak voltages of approximately 32 V during finger tapping (Fig. 6g) and around 45 V during hand tapping (Fig. 6h), while more dynamic movements like elbow motion (Fig. 6i) produced larger voltage swings due to greater mechanical deformation. Activities such as walking (Fig. 6j), running (Fig. 6k), and jumping (Fig. 6l) exhibited increasing output amplitudes, with jumping showing the highest peak voltage of around 120 V, demonstrating the PR-TENG's effectiveness under high-impact mechanical stimuli. These results confirm the suitability of the optimized PR-TENG for wearable and self-powered biomechanical sensing applications.

5. Conclusion

This study successfully demonstrated a facile and cost-effective approach to significantly enhance the electrical output performance of triboelectric nanogenerators by incorporating waste resistor powders into a PVA matrix. The systematic optimization of resistor concentration and value revealed that the PR-TENG with a 0.8 g concentration of 1 $k\Omega$ resistor powder exhibited a superior output of 224.00 V and 7.03 µA, significantly outperforming the plain PVA device. The comprehensive material characterization provided insights into the mechanisms responsible for this enhancement, including improved surface morphology, altered elemental composition, modified crystallinity, and changes in functional groups. The optimized PR-TENG demonstrated its energy harvesting and storage capabilities by effectively charging capacitors, achieving a maximum stored energy of 255.38 µJ. Furthermore, the successful powering of a calculator, direct illumination of LEDs and biomechanical sensor showcased the potential of this technology for self-powered electronic applications. This research not only provides a valuable strategy for improving TENG performance but also offers a sustainable pathway for utilizing electronic waste, contributing to both energy harvesting advancements and environmental responsibility.

CRediT authorship contribution statement

Sebghatullah Amini: Writing – original draft, Visualization, Methodology, Investigation, Conceptualization. Mohan Sankarshan Belur: Writing – original draft, Resources, Project administration, Methodology, Investigation, Conceptualization. Maruthi Dhiren Palahalli Girigowda: Resources, Methodology, Investigation. Ahmed Rumana Farheen Sagade Muktar: Writing – original draft, Visualization, Validation, Methodology, Investigation, Conceptualization. Lingaraj

Adarsh Raj: Writing – original draft, Validation, Methodology, Investigation, Conceptualization. Ankanathappa Sangamesha Madanahalli: Resources, Investigation. S Krishnaveni: Supervision, Project administration, Investigation.

Declaration of Generative AI and AI-assisted technologies in the writing process

During the preparation of this work, the authors used ChatGPT, Paper pal and geminiAI to improve language and readability. After using this tool, the authors reviewed and edited the content as needed and take full responsibility for the content of the publication.

Declaration of Competing Interest

The authors declare that they have no known competing financial interests or personal relationships that could have appeared to influence the work reported in this paper.

Acknowledgements

The authors gratefully acknowledge the funding support received from the Vision Group on Science and Technology (VGST), Government of Karnataka, under Grant for Research Excellence (GRE) scheme with GRD No. 1122, which facilitated the successful execution of the present work. Maruthi Dhiren Palahalli Girigowda acknowledges VGST for providing project assistantship. Rumana Farheen S.M. acknowledges the Council of Scientific and Industrial Research (CSIR), Government of India, for the financial assistance provided under the Research Associate fellowship (File no. 364–4194–9498/2K23/1). Sebghatullah Amini is financially supported by the Indian Council for Cultural Relations (ICCR) scholarship, the government of India. L. Adarsh Raj acknowledges the Karnataka Science and Technology Promotion Society (KSTePS), for providing financial support under DST-Ph.D. fellowship (Award letter No. DST/KSTePS/Ph.D. Fellowship/ MP –05:2023–24/433).

Appendix A. Supporting information

Supplementary data associated with this article can be found in the online version at doi:10.1016/j.sna.2025.116918.

Data availability

Data will be made available on request.

References

- S.T. Ghulam, H. Abushammala, Challenges and opportunities in the management of electronic waste and its impact on human health and environment, Sustainability 15 (2023) 1837.
- [2] C.P. Baldé, R. Kuehr, T. Yamamoto, R. McDonald, E. D'Angelo, S. Althaf, G. Bel, O. Deubzer, E. Fernandez-Cubillo, V. Forti, Glob. eWaste Monit. 2024 (2024).
- [3] K. Parajuly, R. Kuehr, C. Fitzpatrick, Designing behavioural interventions for better e-waste management and the circular economy. Handb. Pro-Environmental Behav. Chang, Edward Elgar Publishing, 2023, pp. 162–183.
- [4] Z.L. Wang, Triboelectric nanogenerators as new energy technology and self-powered sensors-Principles, problems and perspectives, Faraday Discuss. 176 (2014) 447–458.
- [5] L. Xia, H. Zhou, J. Chen, F. Liu, S. Chang, Y. Huang, J. Jiang, K. Dong, Y. Wu, C. Zhang, Human body electrode enabled direct current triboelectric nanogenerator for self-powered wireless human motion and environment monitoring, Adv. Electron. Mater. 10 (2024) 2300713.
- [6] J. Lu, L. Xu, D. Hazarika, C. Zhang, J. Li, J. Wu, K. Zhang, R. Wan, X. Xu, J. Chen, Piezoelectric nanogenerator enabled fully self-powered instantaneous wireless sensor system, Nano Energy 129 (2024) 110022.
- [7] H. Zou, Y. Zhang, L. Guo, P. Wang, X. He, G. Dai, H. Zheng, C. Chen, A.C. Wang, C. Xu, Quantifying the triboelectric series, Nat. Commun. 10 (2019) 1427.
- [8] R.F.S.M. Ahmed, S. Amini, S.M. Ankanathappa, K. Sannathammegowda, Electricity out of electronic trash: triboelectric nanogenerators from discarded smartphone displays for biomechanical energy harvesting, Waste Manag. 178 (2024) 1–11.

- [9] M.U. Bukhari, A. Khan, K.Q. Maqbool, A. Arshad, K. Riaz, A. Bermak, Waste to energy: facile, low-cost and environment-friendly triboelectric nanogenerators using recycled plastic and electronic wastes for self-powered portable electronics, Energy Rep. 8 (2022) 1687–1695.
- [10] B. Zhang, L. He, J. Wang, Y. Liu, X. Xue, S. He, C. Zhang, Z. Zhao, L. Zhou, J. Wang, Self-powered recycling of spent lithium iron phosphate batteries via triboelectric nanogenerator, Energy Environ. Sci. 16 (2023) 3873–3884.
- [11] S. Natarajan, K. Krishnamoorthy, A. Sathyaseelan, V.K. Mariappan, P. Pazhamalai, S. Manoharan, S.-J. Kim, A new route for the recycling of spent lithium-ion batteries towards advanced energy storage, conversion, and harvesting systems, Nano Energy 101 (2022) 107595.
- [12] E. Zhao, K. Jiang, B. Li, X. Liu, F. Zeng, L. Chen, H. Zhang, Z. Zhu, Classification and utilization of waste electronic components based on triboelectric nanogenerator, Nanotechnology 33 (2022) 495401.
- [13] P. Gill, Electrical power equipment maintenance and testing, CRC press, 2016.
- [14] L. Zhang, Z. Xu, A review of current progress of recycling technologies for metals from waste electrical and electronic equipment, J. Clean. Prod. 127 (2016) 19–36.
- [15] E. Hsu, K. Barmak, A.C. West, A.-H.A. Park, Advancements in the treatment and processing of electronic waste with sustainability: a review of metal extraction and recovery technologies, Green. Chem. 21 (2019) 919–936.
- [16] P.M. Ajayan, Bulk metal and ceramics nanocomposites, Nanocomposite Sci. Technol. (2003) 1–75.
- [17] transistors Platt, CharlesEncyclopedia of electronic components volume 1: Resistors, capacitors, inductors, switches, encoders, relays, Encyclopedia of electronic components volume 1: Resistors, capacitors, inductors, switches, encoders, relays, transistors, "O'Reilly Media, Inc.," 2012.
- [18] Y. Li, Y. Luo, H. Deng, S. Shi, S. Tian, H. Wu, J. Tang, C. Zhang, X. Zhang, J. Zha, Advanced dielectric materials for triboelectric nanogenerators: principles, methods, and applications, Adv. Mater. 36 (2024) 2314380.
- [19] F. Maloberti, Resistors, Capacitors, Switches, Analog Des, C. VLSI Syst. (2001) 59–98.
- [20] Y. Fan, S. Li, X. Tao, Y. Wang, Z. Liu, H. Chen, Z. Wu, J. Zhang, F. Ren, X. Chen, Negative triboelectric polymers with ultrahigh charge density induced by ion implantation, Nano Energy 90 (2021) 106574.
- [21] M.P. Kim, D.-S. Um, Y.-E. Shin, H. Ko, High-performance triboelectric devices via dielectric polarization: a review, Nanoscale Res. Lett. 16 (2021) 35.
- [22] R.F.S.M. Ahmed, A.R. Lingaraj, D.H. Neelakantaiah, S.M. Ankanathappa, K. Sannathammegowda, Revolutionizing automobile waste into renewable energy by triboelectric nanogenerators for vehicle safety, Sens. Actuators A Phys. (2025) 116278.
- [23] Z. Peng, X. Xiao, J. Song, A. Libanori, C. Lee, K. Chen, Y. Gao, Y. Fang, J. Wang, Z. Wang, Improving relative permittivity and suppressing dielectric loss of triboelectric layers for high-performance wearable electricity generation, ACS Nano 16 (2022) 20251–20262.
- [24] Y. Feng, Q. Deng, C. Peng, Q. Wu, High dielectric and breakdown properties achieved in ternary BaTiO3/MXene/PVDF nanocomposites with low-concentration fillers from enhanced interface polarization, Ceram. Int. 45 (2019) 7923–7930.
- [25] K. Xiao, W. Wang, K. Wang, H. Zhang, S. Dong, J. Li, Improving triboelectric nanogenerators performance via interface tribological optimization: a review, Adv. Funct. Mater. 34 (2024) 2404744.
- [26] S. Amini, R.F.S.M. Ahmed, S.M. Ankanathappa, M.H.C. Shastry, M. Shivanna, K. Sannathammegowda, Investigating the annealing effects on the performance of polyvinyl alcohol-graphite-based triboelectric nanogenerator, Sens. Actuators A Phys. 372 (2024) 115309.
- [27] A. Uhlir, The potential of semiconductor diodes in high-frequency communications, Proc. IRE 46 (1958) 1099–1115.
- [28] S.A. Shankaregowda, C.B. Nanjegowda, S. Guan, J. Huang, J. Li, R.F.S.M. Ahmed, K. Sannathammegowda, A.M. Boregowda, F. Wang, C. Cheng, A robust triboelectric nanogenerator resistant to humidity and temperature in ambient environment, Phys. Status Solidi (RRL)Rapid Res. Lett. 17 (2023) 2200489.
- [29] J.S. Meena, T.D. Khanh, S.-B. Jung, J.-W. Kim, Self-repairing and energy-harvesting triboelectric sensor for tracking limb motion and identifying breathing patterns, ACS Appl. Mater. Interfaces 15 (2023) 29486–29498.
- [30] R.F. Sagade Muktar Ahmed, S.B. Mohan, S. Madanahalli Ankanathappa, M. Shivanna, P. Viswanathan, H.C.S. Manjunatha, Y.S. Vidya, A. Chandrasekhar, K. Sannathammegowda, Spinach-mediated green synthesized NiFe2O4 nanoparticle-based triboelectric nanogenerator: a smart tollgate controller, ACS Appl. Electron. Mater. 5 (2023) 5885–5897.
- [31] Z.L. Wang, Triboelectric nanogenerators as new energy technology for self-powered systems and as active mechanical and chemical sensors, ACS Nano 7 (2013) 9533–9557.
- [32] R.F. Sagade Muktar Ahmed, A. Kumbarakkara Gangadharan, S. Amini, S. Belur Mohan, S. Madanahalli Ankanathappa, S.Ankanahalli Shankaregowda, K. Sannathammegowda, Economical polypropylene-based triboelectric nanogenerator for self-powered biomechanical sensor application, Phys. Status Solidi 220 (2023) 2200878.
- [33] Y. Liu, J. Mo, Q. Fu, Y. Lu, N. Zhang, S. Wang, S. Nie, Enhancement of triboelectric charge density by chemical functionalization, Adv. Funct. Mater. 30 (2020) 2004714.
- [34] B.P. Hahn, J.W. Long, D.R. Rolison, Something from nothing: enhancing electrochemical charge storage with cation vacancies, Acc. Chem. Res. 46 (2013) 1181–1191.
- [35] J. Zhuang, G.-R. Yu, Effects of surface coatings on electrochemical properties and contaminant sorption of clay minerals, Chemosphere 49 (2002) 619–628.
- [36] X. Chen, J.-K. Tseng, I. Treufeld, M. Mackey, D.E. Schuele, R. Li, M. Fukuto, E. Baer, L. Zhu, Enhanced dielectric properties due to space charge-induced

- interfacial polarization in multilayer polymer films, J. Mater. Chem. C. 5 (2017) 10417–10426
- [37] G. Banhegyi, Interfacial polarization and its diagnostic significance in polymeric composites. in: Interfacial Interact. Polym. Compos, Springer, 1993, pp. 421–430.
- [38] S.F. Mendes, C.M. Costa, C. Caparrós, V. Sencadas, S. Lanceros-Méndez, Effect of filler size and concentration on the structure and properties of poly (vinylidene fluoride)/BaTiO 3 nanocomposites, J. Mater. Sci. 47 (2012) 1378–1388.
- [39] H.M. Otte, Lattice parameter determinations with an x-ray spectrogoniometer by the debye-scherrer method and the effect of specimen condition, J. Appl. Phys. 32 (1961) 1536–1546.
- [40] L. Kong, M. Zhong, W. Shuang, Y. Xu, X.-H. Bu, Electrochemically active sites inside crystalline porous materials for energy storage and conversion, Chem. Soc. Rev. 49 (2020) 2378–2407.
- [41] B. Munirathinam, H. Pydimukkala, N. Ramaswamy, L. Neelakantan, Influence of crystallite size and surface morphology on electrochemical properties of annealed TiO2 nanotubes, Appl. Surf. Sci. 355 (2015) 1245–1253.
- [42] M. Shahbazi, G. Rajabzadeh, A. Rafe, R. Ettelaie, S.J. Ahmadi, Physico-mechanical and structural characteristics of blend film of poly (vinyl alcohol) with biodegradable polymers as affected by disorder-to-order conformational transition, Food Hydrocoll. 71 (2017) 259–269.
- [43] F.K. Konan, B. Hartiti, A. Batan, B. Aka, X-ray diffraction, XPS, and Raman spectroscopy of coated ZnO: Al (1—7 at%) nanoparticles, EJ. Surf. Sci. Nanotechnol. 17 (2019) 163–168.
- [44] A.H.A. Darwesh, S.B. Aziz, S.A. Hussen, Insights into optical band gap identification in polymer composite films based on PVA with enhanced optical properties: structural and optical characteristics, Opt. Mater. (Amst.). 133 (2022) 113007.
- [45] S.B. Dangi, S.Z. Hashmi, U. Kumar, B.L. Choudhary, A.E. Kuznetsov, S. Dalela, S. Kumar, S.N. Dolia, S. Kumar, B.F.I. Sofi, Exploration of spectroscopic, surface morphological, structural, electrical, optical and mechanical properties of biocompatible PVA-GO PNCs, Diam. Relat. Mater. 127 (2022) 109158.
- [46] S.E. Wiberley, R.D. Gonzalez, Infrared spectra of polynuclear aromatic compounds in the CH stretching and out-of-plane bending regions, Appl. Spectrosc. 15 (1961) 174-177
- [47] M. Asemani, A.R. Rabbani, Detailed FTIR spectroscopy characterization of crude oil extracted asphaltenes: curve resolve of overlapping bands, J. Pet. Sci. Eng. 185 (2020) 106618.
- [48] C.N.R. Rao, R. Venkataraghavan, The C= S stretching frequency and the "- N- C= S bands" in the infrared, Spectrochim. Acta Part A Mol. Spectrosc. 45 (1989) 299–305.
- [49] J.O. Dennis, M.F. Shukur, O.A. Aldaghri, K.H. Ibnaouf, A.A. Adam, F. Usman, Y. M. Hassan, A. Alsadig, W.L. Danbature, B.A. Abdulkadir, A review of current trends on polyvinyl alcohol (PVA)-based solid polymer electrolytes, Molecules 28 (2023) 1781
- [50] P. Simon, Y. Gogotsi, Materials for electrochemical capacitors, Nat. Mater. 7 (2008) 845–854.
- [51] C. Zhang, J. Chen, Y. Zhou, C. Zhang, S. Chang, W. Xuan, H. Jin, S. Dong, J. Luo, A battery-less self-powered dual-parameter omnidirectional wireless sensing system based on symmetrical resonant circuit, Nano Energy 125 (2024) 109536.
- [52] S. Chang, J. Chen, F. Liu, J. Chen, C. Zhang, H. Ni, W. Xuan, H. Jin, S. Dong, H. Guo, Harvesting high entropy triboelectric energy using a universal synchronous switching unit for self-powered wireless sensing systems, Nano Energy 131 (2024) 110271.
- [53] D. Jiang, M. Lian, M. Xu, Q. Sun, B. Bin Xu, H.K. Thabet, S.M. El-Bahy, M. M. Ibrahim, M. Huang, Z. Guo, Advances in triboelectric nanogenerator technology—Applications in self-powered sensors, Internet of things, biomedicine, and blue energy, Adv. Compos. Hybrid Mater. 6 (2023) 57.
- [54] M. Lian, J. Sun, D. Jiang, M. Xu, Z. Wu, B. Bin Xu, H. Algadi, M. Huang, Z. Guo, Waterwheel-inspired high-performance hybrid electromagnetic-triboelectric nanogenerators based on fluid pipeline energy harvesting for power supply systems and data monitoring, Nanotechnology 34 (2022) 25401.



Dr. Sankarshan Belur Mohan received his Ph. D. degree in Physics from the University of Mysore, Mysuru in 2018. He is an Assistant Professor at the Department of Physics, The National Institute of Engineering, Mysuru. He secured 3rd rank in B. Sc. from Bangalore University and first rank in M. Sc. With 4 Gold Medals from University of Mysore and a DST INSPIRE Fellow during his Ph. D. His research areas are Materials Science, Compton Scattering, Radiation Physics, Thin films and condensed matter nuclear science.



Maruthi Dhiren Palahalli Girigowda completed his M.Sc. in Physics from Yuvaraja's College, University of Mysore. He is currently working as a Project Assistant in a VGST-funded research project at The National Institute of Engineering (NIE), Mysuru. He is also a research scholar pursuing doctoral studies in the field of Triboelectric Nanogenerators (TENGs). Prior to this, he served as an Assistant Professor of Physics at PES College of Science, Arts and Commerce, Mandya. His research interests include energy harvesting materials, nanogenerators and their applications in self-powered systems.



Dr. Rumana Farheen S. M. is a CSIR Research Associate, she received her Ph.D. in Physics from the Department of Studies in Physics, University of Mysore (UOM), Mysuru, India, in 2024. She was a DST INSPIRE Fellow during her Ph.D. She has secured first rank in M.Sc. and B.Sc. and received seven Gold medals from UOM. Her research interests include the synthesis of nanoparticles, fabrication of flexible triboelectric nanogenerators, self-powered sensors, photoluminescence, and supercapacitors.



Adarsh Raj L. is a Research scholar in Physics from the Department of Studies in Physics, University of Mysore (UOM), Mysuru, India. He is currently a DST KSTePS Fellow, Government of Karnataka. India.



Sebghatullah Amini is a Research scholar in Physics from the Department of Studies in Physics, University of Mysore (UOM), Mysuru, India. Sebghatullah Amini is financially supported by the Indian Council for Cultural Relations (ICCR) scholarship, the government of India.



Dr. Sangamesha M. A. received his M.Sc. degree in Chemistry from the University of Mysore, Mysuru in 2010 and his Ph.D. degree in Chemistry from Visvesvaraya Technological University, Belagavi, India in 2019. He is an Associate Professor at the Department of Chemistry, The National Institute of Engineering, Mysuru. His research interests focus on the synthesis and applications of nano-structured materials, polymer nanocomposites for optoelectronics, supercapacitors, and development of green nanocomposites for agriculture applications.



Dr. Krishnaveni S. received her Ph.D. degree in Physics from the University of Mysore, Mysuru, India, in 2003. Presently, working as a Professor at the Department of Studies in Physics, University of Mysore, Mysuru. She is first ranker in M.Sc. with 4 gold medals and had been CSIR-SRF and CSIR-RA during her research period. Her research interests include Compton profile measurements, fabrication of semiconductor devices and study of radiation effects on them, simulation of biomolecules using molecular dynamics, fabrication, and characterization of self-powered devices such as triboelectric nanogenerators.